ACS APPLIED MATERIALS & INTERFACES

www.acsami.org

Research Article

Laser-Induced Combinatorial Chemotherapeutic, Chemodynamic, and Photothermal Therapy for Hepatocellular Carcinoma Based on Oxaliplatin-Loaded Metal–Organic Frameworks

Run Huang, Weiren Liu, Qinghao Zhang, Guiqi Zhu, Weifeng Qu, Chenyang Tao, Jun Gao, Yuan Fang, Xiutao Fu, Jian Zhou, Yinghong Shi,* Jia Fan,* and Zheng Tang*

Cite This: *ACS Appl. Mater. Interfaces* 2023, 15, 3781−3790

Read Online

ACCESS | Metrics & More | Article Recommendations | Supporting Information

ABSTRACT: The activation of nanoparticles (NPs) in the tumor microenvironment exerts synergistic therapeutic effects with chemotherapy against multiple cancers. In this study, an NP system prepared using biocompatible MIL-100 NPs was studied as an effective vehicle to deliver oxaliplatin for hepatocellular carcinoma treatment. The NPs were coated with polydopamine (PDA) and NH_2-PEGTK-COOH and then loaded with oxaliplatin to create the multi-functional NP Oxa@MIL-PDA-PEGTK. Oxa@MIL-PDA-PEGTK is activated in the tumor microenvironment, causing the generation of cytotoxic reactive oxygen species (ROS) via the Fenton reaction and the release of the loaded oxaliplatin. In addition, under near-infrared (NIR) irradiation, Oxa@MIL-PDA-PEGTK can generate hyperthermia at tumor sites. Moreover, owing to the light-induced activation of the Oxa@MIL-PDA-PEGTK NPs, higher drug delivery efficiency, more precise targeted activation, and reduced off-target toxicity were observed in in vitro and in vivo experiments. Taken together, owing to its improved drug delivery efficiency and multi-functional activities, including the ability for targeted chemotherapy coupled with photothermal and chemodynamic therapy, Oxa@MIL-PDA-PEGTK may serve as a new approach for treating hepatocellular carcinoma.

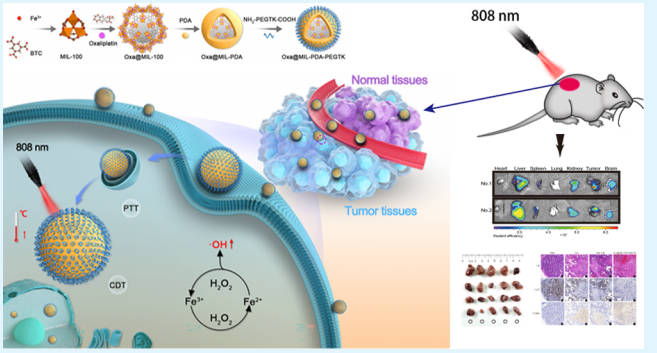

KEYWORDS: *hepatocellular carcinoma, oxaliplatin, nanoparticle, photothermal therapy, chemodynamic therapy*

INTRODUCTION

Hepatocellular carcinoma (HCC) is the fourth most common cause of cancer-related death in the world.[1,2] HCC does not respond to conventional chemotherapeutic agents, limiting their use as first-line therapy in patients with HCC.[3] Only a few patients with advanced HCC receive oxaliplatin-based FOLFOX4 (chemotherapy containing fluorouracil, leucovorin, and oxaliplatin) by infusion as a palliative treatment. However, the FOLFOX4 chemotherapy regimen only provides an overall survival of 6.4 months and progression-free survival of 2.93 months.[4] Therefore, improving the therapeutic efficacy of chemotherapy for patients with HCC is an important clinical goal.

In the past few decades, photothermal therapy (PTT) and chemodynamic therapy (CDT) have emerged as alternative ways to treat tumors, showing high drug delivery efficiency, improved tumor ablation, and minimal adverse effects.[5−7] PTT treatment converts absorbed light into heat, inducing localized hyperthermia and tumor cell death.[8] CDT utilizes the iron-based Fenton reaction to convert intracellular hydrogen peroxide (H_2O_2) to hydroxyl radicals ($^{\cdot}OH$) and reactive oxygen species (ROS), which are cytotoxic to tumor cells.[9−11] Due to the low therapeutic efficacy of CDT,[12] exogenous adjuvants have been developed to enhance the intratumoral Fenton reaction and for improved therapeutic efficacy.[13]

As the efficacy of PTT and CDT depends on the drug concentration, increasing the drug concentration in the tumor is necessary to improve their therapeutic effect. Therefore, a high-efficiency carrier is required to deliver drugs to tumors. Metal−organic frameworks (MOFs) have been widely used in catalysis, drug loading, and drug delivery because of their porosity.[14−17] Iron-based MOFs, such as MIL-100, not only have high porosity to facilitate drug loading but they can degrade in the acidic microenvironment of the tumor, releasing Fe ions that could react with the loaded drugs for CDT. Further, MOFs have been shown to have acceptable in vitro and in vivo cytotoxicity and biodegradability. Wang et al. developed curcumin-loaded MIL-

Received: October 26, 2022
Accepted: January 2, 2023
Published: January 11, 2023

100 nanoparticles (NPs) with a polydopamine-modified hyaluronic acid (HA-PDA) coating on their surface to increase their tumor-targeting ability.[18] Moreover, to increase the aqueous solubility and tumor cell targeting of indocyanine green (ICG), a novel nanoplatform containing ICG-engineered MIL-100 NPs (MOF@HA@ICG NPs) was synthesized, which showed elevated tumor accumulation and photothermal toxicity.[19] In addition, Sheng et al. prepared a nanoplatform based on MIL-100 loaded with chlorin e6 (Ce6) to amplify the Fenton reaction in the tumor microenvironment and enhance the photodynamic effect of CDT.[20] However, although these reports show advances in preparing highly efficient nanoplatforms, a multifunctional NP that combines oxaliplatin-induced chemotherapy and PTT has not yet been reported.

In this study, we loaded oxaliplatin into peroxidase-mimic MIL-100 NPs, which were then coated with PDA and NH_2-PEGTK-COOH to obtain active Oxa@MIL-PDA-PEGTK NPs for use both in vitro and in vivo. These specially formulated Oxa@MIL-PDA-PEGTK NPs were predicted to have three key properties. First, MOF MIL-100 could serve as a peroxidase-like nanozyme and a nanocarrier for oxaliplatin, which would be released under near-infrared (NIR) irradiation. Second, since H_2O_2 accumulates in the tumor microenvironment, the release of Fe^{2+} by the NPs can convert H_2O_2 into hydroxyl radicals ($^{\cdot}OH$ radicals) through the Fenton reaction, inducing tumor cell apoptosis. Third, the PDA coating can convert light into thermal energy, enabling Oxa@MIL-PDA-PEGTK NPs to kill tumor cells through hyperthermia. Both in vitro and in vivo experiments demonstrated that the nanozyme-based chemotherapy/PTT/CDT exerted potent cytotoxicity in liver cancer cells while exerting minimal toxic effects on normal cells. Therefore, these newly designed NPs provide a potentially novel method for effectively ablating tumors in patients with HCC.

EXPERIMENTAL SECTION

Preparation of MIL-100 NPs. MIL-100 NPs were prepared using a previously reported method, with minor adjustments.[21] Briefly, 0.28 g of 1,3,5-benzenetricarboxylic acid and 0.84 g of $FeCl_3{\cdot}6H_2O$ were dissolved in 10 mL of *N*,*N*-dimethylformamide (DMF) in a glass tube and stirred well. The mixture was then placed in a microwave reactor and heated to 130 °C for 5 min. The synthesized MIL-100 NPs were collected by centrifugation at 9000 rpm for 20 min and the pellet was washed three times with DMF.

Preparation of Oxa@MIL NPs. Drug-loaded MIL-100 NPs were prepared by adding oxaliplatin according to the proportion and order during the crystallization process so that the drugs could be embedded relatively separately. MIL-100 NPs (10 mg/mL) and oxaliplatin (30 mg/mL) in dimethylsulfoxide (DMSO) were mixed and stirred for 12 h. Oxaliplatin-loaded Oxa@MIL NPs were collected by centrifugation at 10,000 rpm for 10 min, and the pellet was washed three times with DMSO to remove excess oxaliplatin.

Synthesis of Oxa@MIL-PDA. To synthesize Oxa@MIL-PDA NPs, Oxa@MIL NPs (1 mL) were added to a Tris buffer solution (10 mM, pH 8.5) containing PDA (2.5 mM) and stirred for 0.5 h. The Oxa@MIL-PDA NPs were then washed with distilled water and dried at room temperature.

Preparation of Oxa@MIL-PDA-PEGTK NPs. A solution containing Oxa@MIL NPs (50 mg/mL) and NH_2-PEGTK-COOH (50 mg/mL) was mixed in deionized water with 1-ethyl-3-(3-dimethylaminopropyl) carbodiimide hydrochloride (EDC, 50 mg/mL) and *N*-hydroxylfosuccinimide (NHS, 50 mg/mL) and stirred for 24 h. The mixture was centrifuged at 10,000 rpm for 10 min to obtain Oxa@MIL-PDA-PEGTK NPs and washed three times with deionized water prior to use.

Characterization of the Fabricated NPs. The morphology of the NPs was observed via transmission electron microscopy (TEM). Particle sizes were determined using dynamic light scattering (DLS). The Brunauer−Emmett−Teller (BET) method was used to evaluate the surface area of the NPs. Thermogravimetric analysis (TGA) was performed to evaluate the loading capacity of the NPs. The properties of NPs catalyzing the conversion of hydrogen peroxide to $^{\cdot}OH$ radicals were studied using 3,3′,5,5′-tetramethylbenzidine (TMB) as substrate in the presence of H_2O_2. Color images of the solutions were recorded. To monitor the absorbance of the above aqueous solution, 100 μL of each solution was added to 96-well plates, and the absorbance was measured using a microplate reader (Implen NP80, Germany). Degradation of the material in different pH environments was observed using TEM (FEI, Talos L120, ThermoFisher, USA).

Cumulative Release of Oxaliplatin by NPs. Oxa@MIL-PDA-PEGTK was incubated in solutions at a range of pH values and with different concentrations of H_2O_2. At the indicated time points, the supernatant was collected, and an inductively coupled plasma emission spectrometer was used to determine the concentration of Pt to determine the rate of oxaliplatin leakage.

Photothermal Performance Assessment. The photothermal effect of MIL-PDA-PEGTK NPs at different concentrations was assessed using continuous irradiation with an 808 nm laser (GCSLS-05-007, Daheng New Epoch Technology, Inc., China) for 400 s at a power density of 1 W/cm^2. The temperature change was recorded using an infrared thermographic system (FLIR SC 620, FLIR System, Inc., USA) equipped with a thermocouple (TES 1315, TES Electrical Electronic Corp., China).

Cell Culture. The HCC cell line MHCC97H was purchased from the Cell Bank of the Chinese Academy of Sciences (Shanghai, China). The HCC cell line PLC/PRF/5 and the normal hepatic epithelial cell line L02 were obtained from the American Type Culture Collection. All cell lines were cultured in Dulbecco's modified Eagle's medium supplemented with 10% fetal bovine serum, 100 U/mL penicillin, and 100 mg/mL streptomycin, at 37 °C in a humidified incubator containing 5% CO_2.

Cellular Uptake of NPs. The cellular uptake of NPs was examined using flow cytometry and confocal imaging. First, 4×10^5 cells were seeded in a 24-well plate and incubated overnight. Then, PI@MIL-100 NPs were added to the culture medium to a final concentration of 100 μg/mL and incubated for different time periods. The cells were then analyzed by flow cytometry (BD FACS Aria II, USA). In addition, after incubation with PI@MIL-100 NPs for 4 h, LysoTracker Green (C1047S; Beyotime, China) staining was used to label the lysosomes. Cell nuclei were stained with Hoechst 33342 (C1025, Beyotime, China). The cells were then analyzed using a Leica TCS SP5 confocal microscope.

Intracellular ROS Detection. Intracellular ROS generation induced by Oxa@MIL-PDA-PEGTK was detected using a ROS assay kit (S0033S, Beyotime, China). Cells were seeded in a 24-well plate and incubated overnight, followed by incubation with 100 μg/mL Oxa@MIL-PDA-PEGTK NPs for another 4 h in a 37 °C incubator. The cells were then irradiated with an 808 nm laser for 10 min at a power density of 2.0 W/cm^2. The DCFH-DA ROS probe was diluted 1:1000 in a serum-free medium, added to the cells, and incubated for 20 min, as described in the manufacturer's instructions. After incubation, the images were visualized and recorded using a fluorescence microscope.

Cell Viability Assay. Cancer cells were incubated with 100 μg/mL Oxa@MIL-PDA-PEGTK NPs for 4 h, and either left untreated or exposed to 808 nm laser irradiation for 10 min at a power density of 2.0 W/cm^2. The cells were then stained with an AOPI Staining Solution (CS2-0106, Nexcelom Bioscience) to label live and dead cells and imaged using a fluorescence microscope. For the cell viability assay, 8×10^3 L02 or 6×10^3 PLC/PRF/5 cells were seeded onto each well of a 96-well plate. L02 cells were incubated with MIL-100 NPs at a range of concentrations (0.3125 to 80 μM) for 48 h. PLC/PRF/5 cells were incubated with phosphate-buffered saline (PBS), oxaliplatin, MIL-100 NPs, and Oxa@MIL-PDA-PEGTK NPs, and either left untreated or irradiated with an 808 nm laser for 10 min. Cell viability was examined using a Cell Counting Kit-8 (CCK-8) Dojindo Laboratories, Kyushu, Japan) according to the manufacturer's instructions.

https://doi.org/10.1021/acsami.2c19305
ACS Appl. Mater. Interfaces 2023, 15, 3781−3790

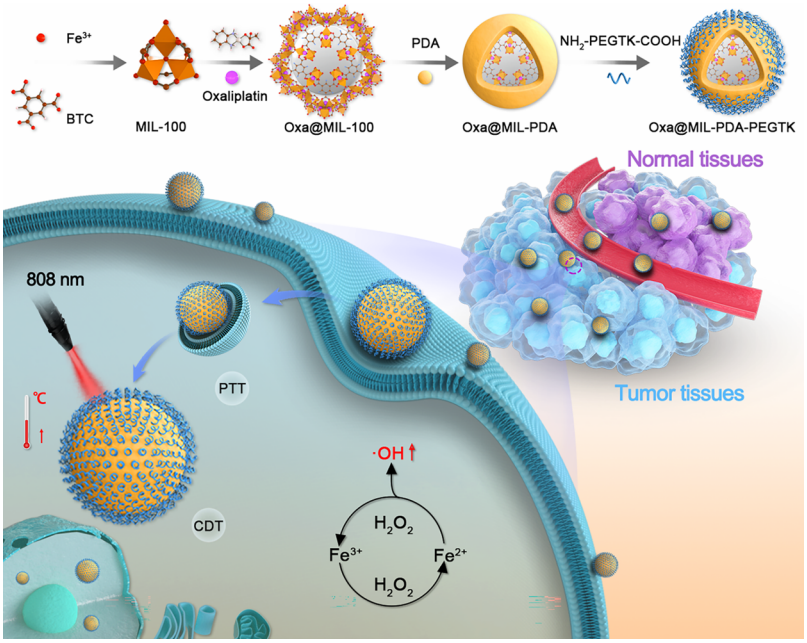

Figure 1. Schematic illustration of the synthesis and therapeutic mechanism of Oxa@MIL-PDA-PEGTK NPs.

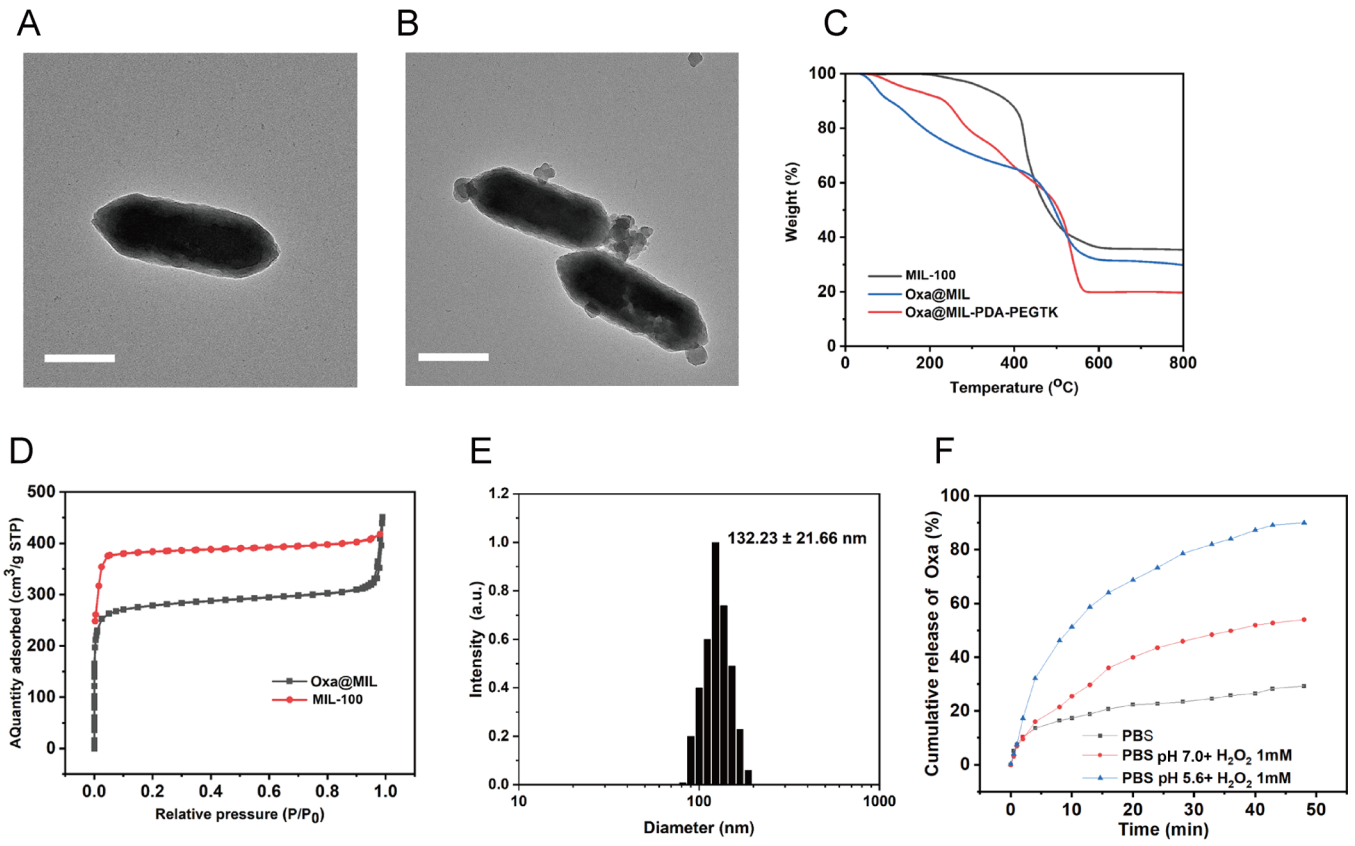

Figure 2. Physicochemical characteristics of the MIL-100-based nanoparticles. (A) TEM images of MIL-100 NPs. (B) TEM images of MIL-PDA-PEGTK NPs. Scale bars represent 100 nm. (C) TGA isotherms of MIL-100 and MIL-PDA-PEGTK. (D) Nitrogen absorption curves of MIL-100 and Oxa@MIL. (E) DLS particle size distribution of MIL-PDA-PEGTK. (F) Release profile of oxaliplatin from Oxa@MIL-PDA-PEGTK at different H_2O_2 concentration. BPS, phosphate buffer.

Xenograft Tumor Models. Male BALB/C-nu mice (5 weeks old) were purchased from Shanghai Jihui Laboratory Animal Care Co., Ltd. and bred in a sterile animal facility at Fudan University. PLC/PRF/5 cells (1×10^6) were diluted in 100 μL PBS and injected subcutaneously into the right axillary region of the mice. All mice were fed in a specific pathogen-free environment and all experimental procedures rigorously complied with the Guide for the Care and Use of Laboratory Animals.

Biodistribution of NPs and Photothermal Imaging. PLC/PRF/5 tumor-bearing mice were used to examine the biodistribution of NPs in vivo. When the tumor size reached 250 mm^3, Cy7@MIL-100

https://doi.org/10.1021/acsami.2c19305
ACS Appl. Mater. Interfaces 2023, 15, 3781−3790

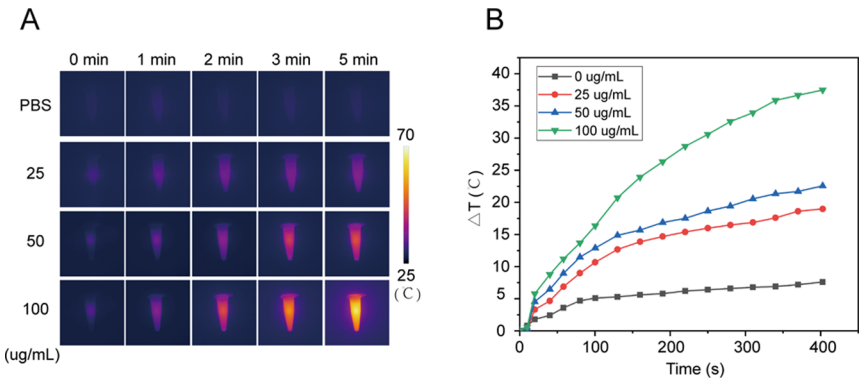

Figure 3. Photothermal characteristics of the nanoparticles. (A) Infrared thermal images of MIL-PDA-PEGTK with continuous 808 nm wave laser at different concentrations for 5 min at a density power of 1 W/cm^2. (B) Temperature elevation of MIL-PDA-PEGTK NPs at different concentrations. PBS, phosphate buffer.

NPs were injected into the tail vein at a dose of 5 mg/kg. Six hours after injection, the major organs, including the heart, liver, spleen, lungs, kidneys, and tumors, were harvested and imaged using an Inter-Vehicle Information System (IVIS, PerkinElmer, USA). The organs were observed using excitation and emission wavelengths of 750 and 788 nm, respectively. Similarly, tumor-bearing mice were injected with PBS and Oxa@MIL-PDA-PEGTK NPs (5 mg/kg), and the xenograft tumors were irradiated with an 808 nm laser (2 W/cm^2) for 5 min. Six hours after injection, thermal images and temperatures were recorded every minute using a photothermal sensor.

Tumor Growth Inhibition In Vivo. When the tumor volume reached 150 mm^3, PLC/PRF/5 tumor-bearing mice were randomly divided into five groups: PBS, oxaliplatin, MIL-100, Oxa@MIL-PDA-PEGTK without laser irradiation, and Oxa@MIL-PDA-PEGTK with laser irradiation (808 nm, 2 W/cm^2, 5 min). At 6 and 12 days after tumor cell inoculation, oxaliplatin was administered at a dose of 2 mg/kg, while the NPs were administered at a dose of 20 mg/kg, which was equivalent to 2 mg/kg oxaliplatin (the drug loading rate of the NPs was 10%). Laser irradiation was given 6 h after injection of Oxa@MIL-PDA-PEGTK NPs. The tumor size and body weight were measured every 3 days. Tumor volumes were calculated using the formula: Tumor volume = 0.5 × width × width × length. All mice were sacrificed on day 23, and the peripheral blood, tumors, and main organs (heart, liver, spleen, lungs, and kidneys) were collected for further analysis.

Biochemical Examination and Pathological Analysis of Mice. The peripheral blood was collected in 1.5 mL centrifuge tubes, stored at 4 °C for 2 h, and centrifuged at 9000 rpm for 5 min to separate the serum. An automatic ADVIA XPT system (Siemens Healthcare Diagnostics Inc., USA) was used to analyze the levels of albumin (ALB), total protein (TP), alanine transaminase (ALT), aspartate aminotransferase (AST), alkaline phosphatase, cholinesterase, lactate dehydrogenase (LDH), creatine kinase (CK), blood urea nitrogen (BUN), blood uric acid (BUA), and glucose in the serum samples.

The tumors and main organs were fixed in 4% paraformaldehyde and paraffin sections were prepared. Hematoxylin and eosin (H&E) staining was performed to determine pathological changes in the main organs (heart, liver, spleen, lungs, and kidneys) to evaluate overall cytotoxicity. Immunohistochemical analysis using Ki-67 staining was also performed according to a previously published paper[22] to determine the proliferation of the tumors. Finally, a TUNEL assay kit (C1091, Beyotime, China) was used to determine apoptosis in tumors, as described in the manufacturer's instructions.

Statistical Analysis. All experimental data are presented as the mean ± standard deviation or mean ± standard error. Two-tailed unpaired Student's *t*-test or one-way analysis of variance (ANOVA) were performed to analyze the data and determine statistical significance. Repeated measures by ANOVA were performed to analyze tumor volumes and body weights. All statistical analyses were performed using SPSS 24.0 and GraphPad Prism 8.0 software. In the present study, *p*-values less than 0.05 were considered statistically significant.

RESULTS AND DISCUSSION

Characterization of NPs. Synthesis of MIL-100 and MIL-PEGTK NPs are described in the methods and summarized in Figure 1. TEM images in Figures 2A,B demonstrate the uniform polyhedral morphology of MIL-100 and MIL-PDA-PEGTK, with nanoscale dimensions indicated. After PDA and PEGTK functionalization, the MIL-100 surface became rougher and the diameter of the NPs increased. The MIL-100, Oxa@MIL, and Oxa@MIL-PDA-PEGTK NPs showed approximately 64.39, 69.73, and 80.23% mass loss (200−800 °C) respectively, compared to the parent MIL-100 NPs (Figure 2C), which indicates that approximately 5.34% oxaliplatin was absorbed into the MIL-100 NPs. Figure 2D demonstrates that both exhibited a typical type I N_2 absorption−desorption isotherm, which is one of the major characteristics of microporous materials. The surface area of the parent MIL-100, determined by the BET method, was 1176 m^2/g, whereas that of Oxa@MIL decreased to 563 m^2/g after oxaliplatin loading. Furthermore, the corresponding pore volumes of the MIL-100 and purified Oxa@MIL NPs were 0.751 and 0.716 cm^3/g, respectively. The sharp reduction in the BET surface area and pore volume indicates the presence of abundant oxaliplatin molecules inside the MIL-100 NPs. In addition, DLS confirmed that the diameter of the MIL-PDA-PEGTK NPs was approximately 132.23 nm (Figure 2E).

The release profile of oxaliplatin from Oxa@MIL-PDA-PEGTK incubated in PBS, H_2O_2, or acidic H_2O_2 solutions was determined. As illustrated in Figure 2F, the release of oxaliplatin from Oxa@MIL-PDA-PEGTK NPs was sustained for at least 48 min. Approximately 90% of the oxaliplatin was released from the Oxa@MIL-PDA-PEGTK NPs within 48 min of immersion in an acidic H_2O_2 solution (1 mM). However, this release of oxaliplatin was reduced to 54 and 29.3% when immersed in either H_2O_2 or PBS, respectively. Because MIL-100 NPs can degrade in the acidic microenvironment of tumors, TEM analysis was used to monitor the degradation of MOF after a 3 h incubation in PBS at either pH 6.5 or pH 5.6. Oxa@MIL-PDA-PEGTK was significantly degraded at pH 5.6 (Figure S1), which provides further evidence to confirm that oxaliplatin is released from Oxa@MIL-PDA-PEGTK at pH 5.6.

Next, the photothermal effect was examined under 808 nm NIR laser radiation. Figure 3 indicates a rapid increase in temperature, approximately 35 °C, was observed in the MIL-PDA-PEGTK NPs (100 μg/mL) solution after NIR radiation for 300 s. Similarly, the temperatures of the 25 and 50 μg/mL

https://doi.org/10.1021/acsami.2c19305
ACS Appl. Mater. Interfaces 2023, 15, 3781−3790

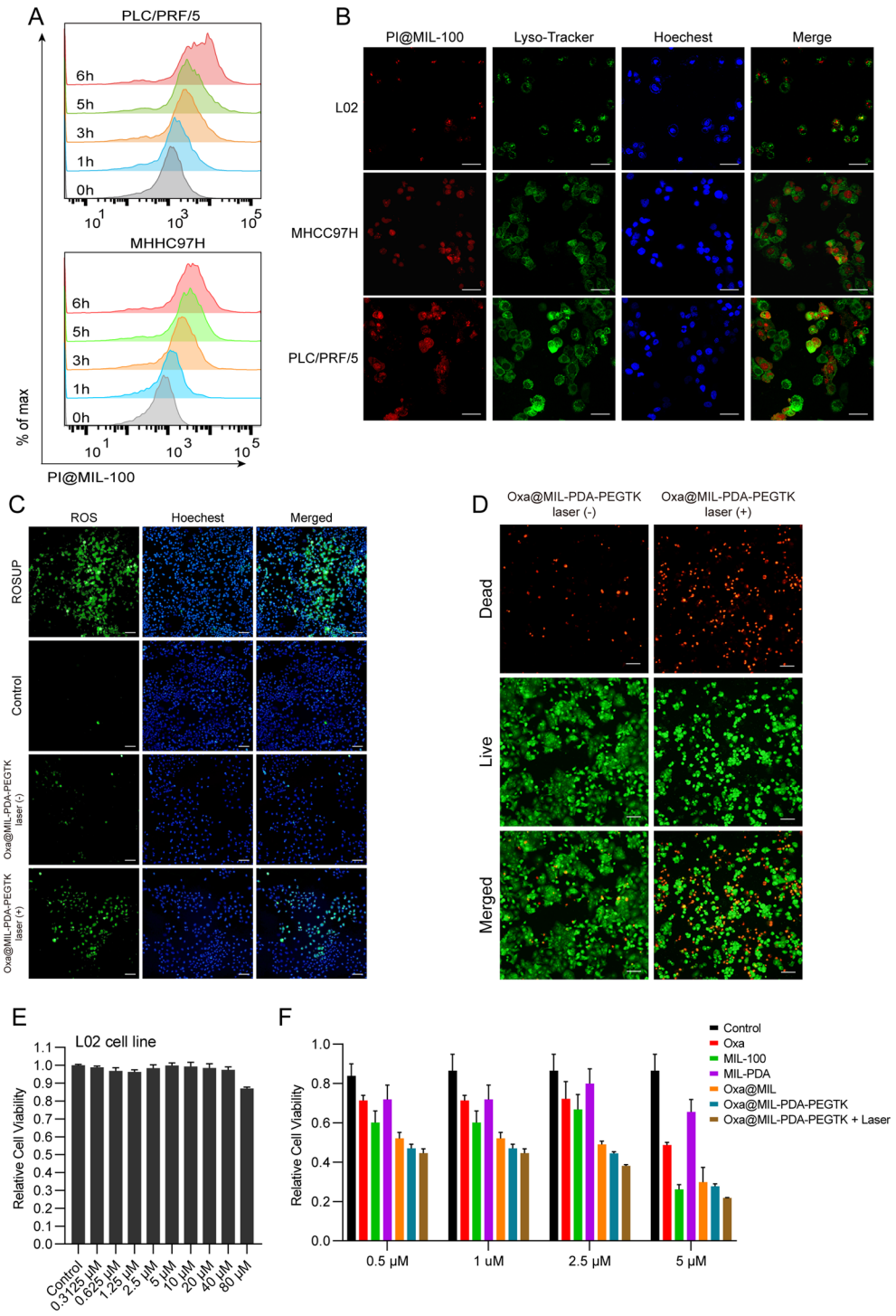

Figure 4. The intracellular distribution and in vitro cytotoxicity of the nanoparticles. (A) The flow cytometry analysis of PI@MIL-100 uptake by liver cancer cell lines at different time points. (B) Immunofluorescence images of normal hepatic epithelial cells and liver cancer cells treated with PI@MIL-100 for 4 h (scale bar is 100 μm). (C) Detection of ROS levels of PLC/PRF/5 cells treated with Oxa@MIL-PDA-PEGTK with or without 808 nm laser irradiation (scale bar is 100 μm). (D) PLC/PRF/5 cells were treated with Oxa@MIL-PDA-PEGTK for 4 h and then irradiated with 808 nm laser. Microscopy images were taken after stained with LIVE/DEAD kit (scale bar is 100 μm). (E) Cell viability of L02 cells treated with Oxa@MIL-PDA-PEGTK at different concentrations. (F) Cell viability of PLC/PRF/5 cells treated with different NPs.

MIL-PDA-PEGTK solutions also increased rapidly. In contrast, negligible temperature changes were observed in the PBS solution. Additionally, the photothermal stability of the MIL-PDA-PEGTK NPs was examined using the photothermal performance cycle. Five cycles of laser irradiation had no observable impact on the temperature curve (Figure S2), indicating that constant irradiation with NIR light had no apparent effect on the photothermal conversion properties of the MIL-PDA-PEGTK NPs. These data demonstrate the excellent photothermal conversion efficacy of MIL-PDA-PEGTK NPs.

https://doi.org/10.1021/acsami.2c19305
ACS Appl. Mater. Interfaces 2023, 15, 3781−3790

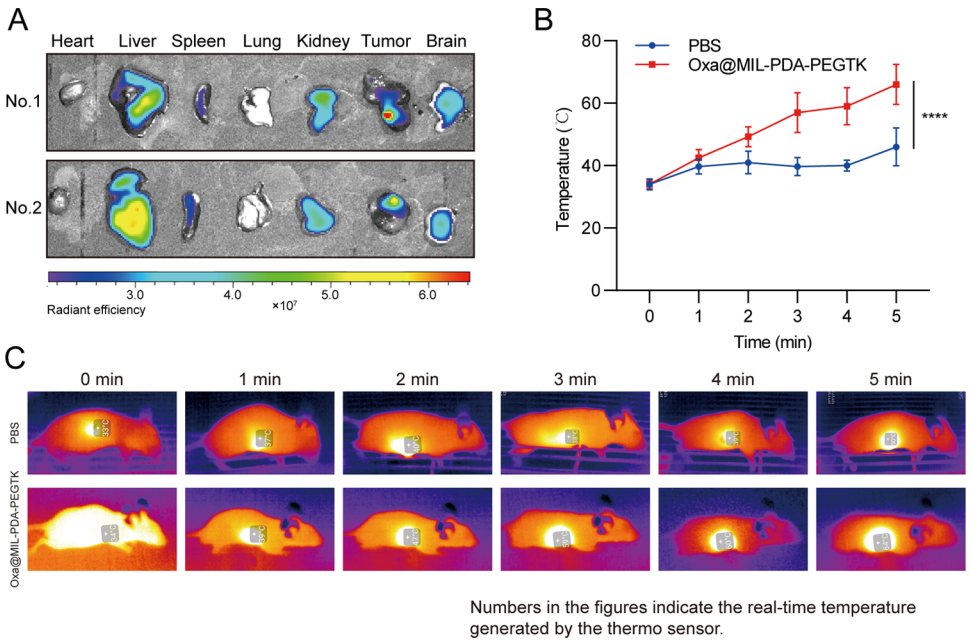

Figure 5. The in vivo distribution and photothermal effect of the nanoparticles. (A) Ex vivo fluorescence signals of NPs distribution in mice treated with Cy7@MIL-100 via tail vein injection. (B) Temperature change of irradiated tumors with 808 nm laser at different time. (C) Infrared thermal images of tumor-bearing mice 6 h after injection of PBS or Oxa@MIL-PDA-PEGTK under different irradiation time.

The catalytic activity of MOF NPs in the presence of a low concentration of H_2O_2 was evaluated using the chromogenic reaction of TMB. The MIL-100 NPs catalyze H_2O_2 hydrolysis via the Fenton reaction to produce hydroxyl radicals, which further oxidize the colorless TMB solution to form a blue solution with two absorption peaks at 370 and 650 nm. The ·OH radical production by MIL-100 NPs was evaluated at different concentrations of NPs at pH 5.6. Figure S3 demonstrates that MIL-100 NPs generate hydroxyl radicals through the Fenton reaction and that the concentration of hydroxyl radicals increased as the concentration of MIL-100 NPs increased.

Intracellular Distribution and Targeted Toxicity of NPs in Tumor Cells. To monitor the uptake of the NPs by cancer cells, two hepatocellular carcinoma cell lines (PLC/PRF/5 and MHCC97H) were incubated with propidium iodide (PI)-loaded MIL-100 (PI@MIL-100) NPs and then subjected to analysis by flow cytometry. PI@MIL-100 NPs were absorbed by the cancer cells in a time-dependent manner (Figure 4A). In addition, the intracellular distribution of PI@MIL-100 NPs was visualized using confocal microscopy. More NPs were absorbed by cancer cells than by the normal hepatic cell line L02 (Figure 4B), implying a low probability of off-target delivery to normal cells that might cause toxic side effects. Further, most PI@MIL-100 NPs accumulated in the nucleus, with little accumulation in lysosomes, indicating that the NPs may escape lysosomal degradation. NP accumulation in the nucleus is also favorable for delivery of the released oxaliplatin. Oxaliplatin is a platinum compound that forms both inter- and intra-strand cross-links with DNA, inhibiting replication and transcription, and causing cell death.[23] The accumulation of NPs in the nucleus provides targeted release of oxaliplatin directly to the DNA, where it can exert its cytotoxic effects on cancer cells.

Treatment of tumor cells without NPs or with Oxa@MIL-PDA-PEGTK NPs only induced weak green fluorescence compared to similarly treated cells exposed to NIR irradiation (Figure 4C), indicating that Oxa@MIL-PDA-PEGTK induced a strong free radical response upon NIR treatment. Staining of live/dead cells with AOPI demonstrated that Oxa@MIL-PDA-PEGTK exhibited higher cytotoxicity in tumor cells upon NIR irradiation (Figure 4D), consistent with the observation that more oxaliplatin was released from the NPs due to ROS generation with NIR irradiation. These data indicate that NIR irradiation of Oxa@MIL-PDA-PEGTK NPs significantly increased ROS generation via the Fenton reaction and accelerated the necrosis of tumor cells.

To examine the tumor-specific cytotoxicity of Oxa@MIL-PDA-PEGTK NPs in vitro, tumor cells were incubated with different NPs followed by measurement of apoptosis using the CCK-8 apoptosis assay. Notably, negligible cytotoxicity of MIL-100 NPs was observed on the normal hepatic cell line L02, even at higher concentrations (80 μM; Figure 4E); this concentration corresponded to the content of free oxaliplatin that could be loaded onto the NPs. However, even at low concentrations (0.5 μM), tumor cells were more sensitive to treatment with NPs, especially Oxa@MIL-PDA-PEGTK NPs plus NIR irradiation, compared to oxaliplatin alone (Figure 4F). Moreover, Oxa@MIL-PDA-PEGTK NPs plus NIR irradiation resulted in stronger cytotoxicity than Oxa@MIL-PDA-PEGTK NPs alone at 2.5 and 5.0 μM (Figure 4F). These results demonstrate that tumor cells are more susceptible to treatment with Oxa@MIL-PDA-PEGTK NPs, while normal cells tend to be more resistant to NP treatment.

Improved Tumor Cytotoxicity and Reduced Adverse Side Effects after NP Treatment. To observe the in vivo biodistribution of NPs in tumor-bearing mice, the fluorochrome Cy7 was loaded onto MIL-100 NPs (Cy7@MIL-100) and administered to animals via tail vein injection. Eight hours later, the mice were sacrificed and imaging using an IVIS system revealed Cy7@MIL-100 NP accumulation in the xenograft tumor, liver, and kidneys (Figure 5A). Most therapeutic agents are metabolized in the liver and filtered out by the kidneys before being excreted from the body. Remarkably, a strong fluorescence signal was observed in the xenograft tumor tissue, demonstrating the improved targeting ability of the NPs. As noted in previously

https://doi.org/10.1021/acsami.2c19305
ACS Appl. Mater. Interfaces 2023, 15, 3781−3790

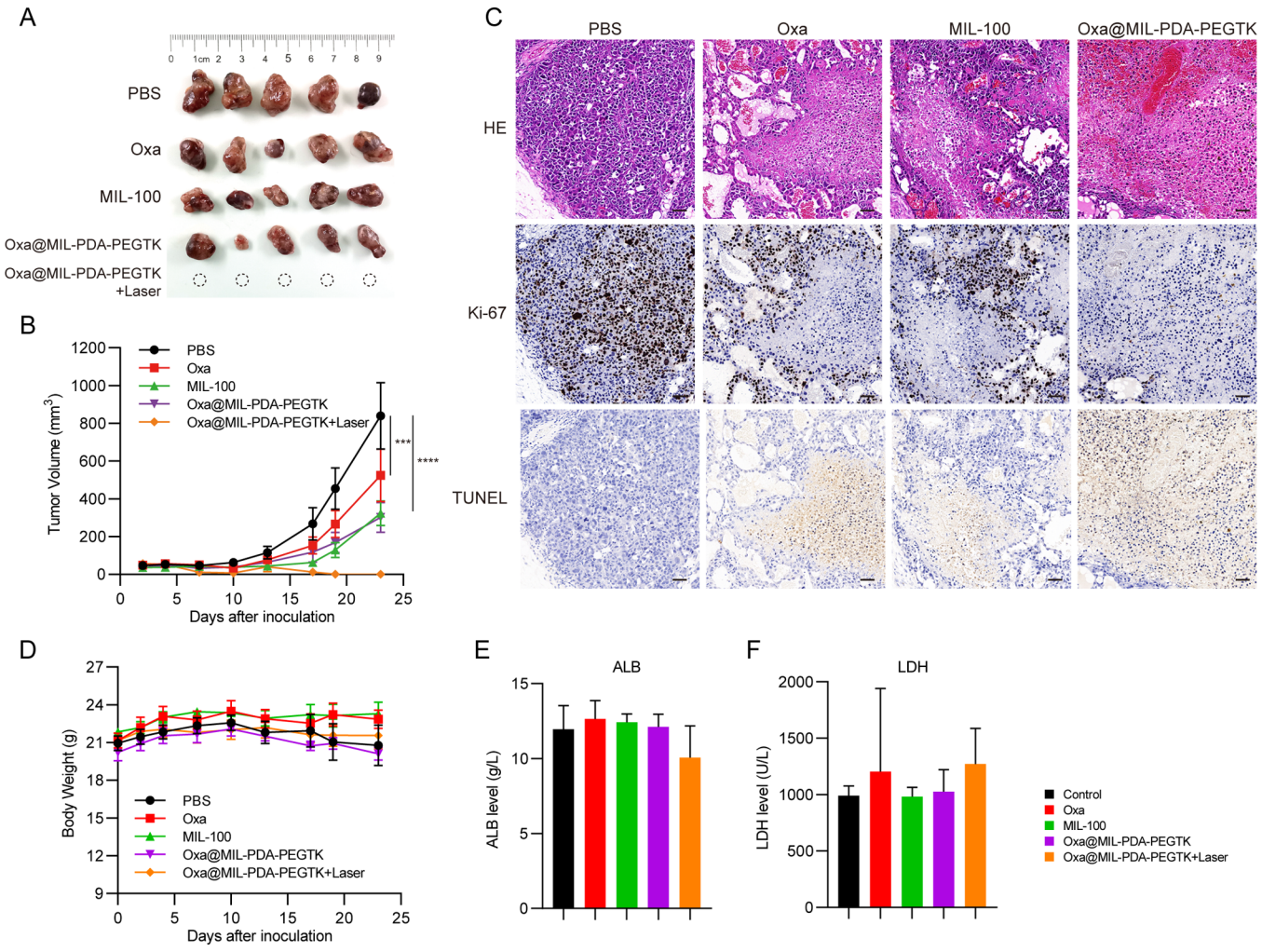

Figure 6. Enhanced in vivo therapeutic effect and reduced side effects. (A) Gross images of resected tumors from PLC/PRF/5-bearing mice at day 23. (B) Tumor volume curves with indicated treatments (mean ± SEM). (C) Body weight changes of nude mice with indicated treatments (mean ± SEM). (D) Microscopy images of tumors with H&E staining, Ki-67 staining, and TUNEL staining after indicated treatments. (E) Biochemical marker analysis of ALB and LDH levels in blood serum of mice with indicated treatments. ALB, albumin; LDH, lactate dehydrogenase.

published papers, the accumulation of NPs in the tumor tissue is highly associated with the enhanced therapeutic effect of NPs.[24,25]

Next, we examined the ability of NPs to transform light into heat energy at tumor sites. PBS or Oxa@MIL-PDA-PEGTK NPs were injected into the tail vein of PLC/PRF/5 tumor-bearing mice. Six hours after injection, xenograft tumors were exposed to irradiation using an 808 nm laser and photographed with a thermal sensor. Within 5 min of NIR irradiation, the temperature at the tumor site was significantly higher in mice injected with NPs compared to PBS (Figures 5B,C). The time-dependent photothermal therapy assay demonstrated that the Oxa@MIL-PDA-PEGTK NPs generated hyperthermia in the tumor after 808 nm NIR laser irradiation, consistent with NPs being located mainly inside the tumors. Compared with the mild temperature change in the PBS group, the rapid temperature increase mediated by NPs demonstrates their potential ability to kill tumor cells without damaging normal tissues.

We then performed in vivo assays to examine the therapeutic effects of the oxaliplatin-loaded NPs. BALB/C nude mice were divided into five groups: PBS, oxaliplatin, MIL-100, Oxa@MIL-PDA-PEGTK without NIR, and Oxa@MIL-PDA-PEGTK with NIR irradiation. As expected, oxaliplatin, a platinum-based compound used to treat malignant tumors, especially colon cancer,[26] significantly suppressed liver tumor growth (Figure 6A,B). In comparison, MIL-100 and Oxa@MIL-PDA-PEGTK NPs also exhibited minor inhibitory effects, which was consistent with the results of the in vitro experiments (Figure 6A,B). However, combined treatment with Oxa@MIL-PDA-PEGTK plus NIR irradiation completely ablated subcutaneous tumors and inhibited further recurrence (Figure 6A,B). Moreover, decreased staining with Ki-67, a cell proliferation marker, and increased apoptosis were observed in tumors treated with Oxa@MIL-PDA-PEGTK NPs (Figure 6C).

In the present study, negligible body weight loss was observed in all five groups, revealing the good biocompatibility of these NPs (Figure 6D). To examine whether there were morphological changes induced by treatment with oxaliplatin and NPs, H&E staining was performed on major organs, including the heart, liver, spleen, lungs, and kidneys. As shown in Supplementary Figure S4, severe pulmonary congestion and tracheal secretion were observed in oxaliplatin-treated mice, although oxaliplatin significantly suppressed tumor growth (yellow and blue arrows). In addition, oxaliplatin treatment induced sporadic edema surrounding the interlobular arteries of the kidneys (black arrow). In contrast, negligible pathological

https://doi.org/10.1021/acsami.2c19305
ACS Appl. Mater. Interfaces 2023, 15, 3781−3790

changes were detected in the major organs of mice that received NPs. Additionally, peripheral blood was collected from all mice and subjected to biochemical assays. No obvious toxic effects on liver function, cardiac function, and renal function were observed (Figure 6E,F and Supplementary Figure S5), as evidenced by the comparable ALB, TP, ALT, AST, LDH, CK, BUN, and BUA levels across groups.

Because liver tumors are localized inside the upper abdomen, light-driven PTT and CDT regimens may be inappropriate for their treatment. However, interstitial photodynamic therapy, using single or multiple laser fibers inserted into the targeted tissues under imaging guidance, is well suited for patients with deep or large tumors, such as prostate cancer, pancreatic cancer, and brain cancer.[27] Therefore, this study suggests that light-based NP treatment, coupled with laser fibers for targeted light delivery, may be applicable for the ablation of liver tumors and could be beneficial for patients with HCC.

Because of the poor response to chemotherapeutic agents in liver cancer, chemotherapy is usually prescribed for patients with unresectable tumors or those who do not respond to targeted therapies and other local treatments, such as ablation or embolization.[28,29] The most commonly used chemotherapy drugs for liver cancer include oxaliplatin, gemcitabine, doxorubicin, and 5-fluorouracil.[29] Among these chemotherapeutic agents, the platinum-based chemotherapy drug oxaliplatin has stronger DNA binding affinity and tumor-suppressive effects than the related compounds cisplatin or carboplatin.[26] The primary toxic side effects of oxaliplatin treatment include neurotoxicity and myelosuppression, while minor nephrotoxicity and cardiotoxicity have also been observed.[23,30,31] Similar to the minor side effects of unconjugated oxaliplatin, oxaliplatin-loaded NPs also exhibited minimal adverse effects on tumor-bearing mice in this study, as illustrated by the lack of pathological changes in major organs and the levels of key biochemical markers.

CONCLUSIONS

In summary, we designed an NP-based drug delivery system that could efficiently deliver chemotherapeutic agents to tumors. In vitro experiments demonstrated Fe^{2+} release at tumor sites increased ROS generation in laser-irradiated cancer cells, while exhibiting low cytotoxicity in non-cancerous cells. In addition, these findings were confirmed by in vivo studies, which indicated that laser irradiation triggered a Fenton reaction in the tumor microenvironment, exhibiting a proficient tumor inhibition with minimal adverse effects. We believe that this study may pave the way for designing novel nanoplatforms responsive to the tumor microenvironment, which will achieve enhanced treatment effects in patients with HCC in the future.

ASSOCIATED CONTENT

Supporting Information

The Supporting Information is available free of charge at https://pubs.acs.org/doi/10.1021/acsami.2c19305.

TEM images of degradation of MOF, heating and cooling curves of MIL-PDA-PEGTK, catalytic performance, histology study of multiple organs, and mouse blood serum analysis (PDF)

AUTHOR INFORMATION

Corresponding Authors

Yinghong Shi − *Department of Liver Surgery and Transplantation, Liver Cancer Institute, Zhongshan Hospital, Fudan University, and Key Laboratory of Carcinogenesis and Cancer Invasion of Ministry of Education, Shanghai 200032, China; Research Unit of Bench and Clinic Research for Liver Cancer Recurrence and Metastasis, Chinese Academy of Medical Sciences (No. 2019RU050), Shanghai 200032, China*; Phone: +86-21-64041990-3233; Email: shi.yinghong@zs-hospital.sh.cn; Fax: +86-21-64037181

Jia Fan − *Department of Liver Surgery and Transplantation, Liver Cancer Institute, Zhongshan Hospital, Fudan University, and Key Laboratory of Carcinogenesis and Cancer Invasion of Ministry of Education, Shanghai 200032, China; Research Unit of Bench and Clinic Research for Liver Cancer Recurrence and Metastasis, Chinese Academy of Medical Sciences (No. 2019RU050), Shanghai 200032, China*; Phone: +86-21-64041990; Email: fan.jia@zs-hospital.sh.cn; Fax: +86-21-64037181

Zheng Tang − *Department of Liver Surgery and Transplantation, Liver Cancer Institute, Zhongshan Hospital, Fudan University, and Key Laboratory of Carcinogenesis and Cancer Invasion of Ministry of Education, Shanghai 200032, China; Research Unit of Bench and Clinic Research for Liver Cancer Recurrence and Metastasis, Chinese Academy of Medical Sciences (No. 2019RU050), Shanghai 200032, China*; orcid.org/0000-0003-0256-4494; Phone: +86-21-64041990-8612; Email: tang.zheng@zs-hospital.sh.cn

Authors

Run Huang − *Department of Liver Surgery and Transplantation, Liver Cancer Institute, Zhongshan Hospital, Fudan University, and Key Laboratory of Carcinogenesis and Cancer Invasion of Ministry of Education, Shanghai 200032, China; Research Unit of Bench and Clinic Research for Liver Cancer Recurrence and Metastasis, Chinese Academy of Medical Sciences (No. 2019RU050), Shanghai 200032, China*

Weiren Liu − *Department of Liver Surgery and Transplantation, Liver Cancer Institute, Zhongshan Hospital, Fudan University, and Key Laboratory of Carcinogenesis and Cancer Invasion of Ministry of Education, Shanghai 200032, China; Research Unit of Bench and Clinic Research for Liver Cancer Recurrence and Metastasis, Chinese Academy of Medical Sciences (No. 2019RU050), Shanghai 200032, China*

Qinghao Zhang − *East China University of Science and Technology, Shanghai 200237, China*

Guiqi Zhu − *Department of Liver Surgery and Transplantation, Liver Cancer Institute, Zhongshan Hospital, Fudan University, and Key Laboratory of Carcinogenesis and Cancer Invasion of Ministry of Education, Shanghai 200032, China; Research Unit of Bench and Clinic Research for Liver Cancer Recurrence and Metastasis, Chinese Academy of Medical Sciences (No. 2019RU050), Shanghai 200032, China*

Weifeng Qu − *Department of Liver Surgery and Transplantation, Liver Cancer Institute, Zhongshan Hospital, Fudan University, and Key Laboratory of Carcinogenesis and Cancer Invasion of Ministry of Education, Shanghai 200032, China; Research Unit of Bench and Clinic Research for Liver Cancer Recurrence and Metastasis, Chinese Academy of*

Medical Sciences (No. 2019RU050), Shanghai 200032, China

Chenyang Tao − *Department of Liver Surgery and Transplantation, Liver Cancer Institute, Zhongshan Hospital, Fudan University, and Key Laboratory of Carcinogenesis and Cancer Invasion of Ministry of Education, Shanghai 200032, China; Research Unit of Bench and Clinic Research for Liver Cancer Recurrence and Metastasis, Chinese Academy of Medical Sciences (No. 2019RU050), Shanghai 200032, China*

Jun Gao − *Department of Liver Surgery and Transplantation, Liver Cancer Institute, Zhongshan Hospital, Fudan University, and Key Laboratory of Carcinogenesis and Cancer Invasion of Ministry of Education, Shanghai 200032, China; Research Unit of Bench and Clinic Research for Liver Cancer Recurrence and Metastasis, Chinese Academy of Medical Sciences (No. 2019RU050), Shanghai 200032, China*

Yuan Fang − *Department of Liver Surgery and Transplantation, Liver Cancer Institute, Zhongshan Hospital, Fudan University, and Key Laboratory of Carcinogenesis and Cancer Invasion of Ministry of Education, Shanghai 200032, China; Research Unit of Bench and Clinic Research for Liver Cancer Recurrence and Metastasis, Chinese Academy of Medical Sciences (No. 2019RU050), Shanghai 200032, China*

Xiutao Fu − *Department of Liver Surgery and Transplantation, Liver Cancer Institute, Zhongshan Hospital, Fudan University, and Key Laboratory of Carcinogenesis and Cancer Invasion of Ministry of Education, Shanghai 200032, China; Research Unit of Bench and Clinic Research for Liver Cancer Recurrence and Metastasis, Chinese Academy of Medical Sciences (No. 2019RU050), Shanghai 200032, China*

Jian Zhou − *Department of Liver Surgery and Transplantation, Liver Cancer Institute, Zhongshan Hospital, Fudan University, and Key Laboratory of Carcinogenesis and Cancer Invasion of Ministry of Education, Shanghai 200032, China; Research Unit of Bench and Clinic Research for Liver Cancer Recurrence and Metastasis, Chinese Academy of Medical Sciences (No. 2019RU050), Shanghai 200032, China*

Complete contact information is available at: https://pubs.acs.org/10.1021/acsami.2c19305

Notes

The authors declare no competing financial interest.

■ ACKNOWLEDGMENTS

The authors are thankful to the National Natural Science Foundation of China (82003084 and 92042301).

■ REFERENCES

(1) Villanueva, A. Hepatocellular Carcinoma. *N. Engl. J. Med.* **2019**, *380*, 1450−1462.

(2) Siegel, R. L.; Miller, K. D.; Jemal, A. Cancer statistics, 2020. *CA, Cancer J. Clin.* **2020**, *70*, 7−30.

(3) Gordan, J. D.; Kennedy, E. B.; Abou-Alfa, G. K.; Beg, M. S.; Brower, S. T.; Gade, T. P.; Goff, L.; Gupta, S.; Guy, J.; Harris, W. P.; Iyer, R.; Jaiyesimi, I.; Jhawer, M.; Karippot, A.; Kaseb, A. O.; Kelley, R. K.; Knox, J. J.; Kortmansky, J.; Leaf, A.; Remak, W. M.; Shroff, R. T.; Sohal, D. P. S.; Taddei, T. H.; Venepalli, N. K.; Wilson, A.; Zhu, A. X.; Rose, M. G. Systemic Therapy for Advanced Hepatocellular Carcinoma: ASCO Guideline. *J. Clin. Oncol.* **2020**, *38*, 4317−4345.

(4) Qin, S.; Bai, Y.; Lim, H. Y.; Thongprasert, S.; Chao, Y.; Fan, J.; Yang, T. S.; Bhudhisawasdi, V.; Kang, W. K.; Zhou, Y.; Lee, J. H.; Sun, Y. Randomized, multicenter, open-label study of oxaliplatin plus fluorouracil/leucovorin versus doxorubicin as palliative chemotherapy in patients with advanced hepatocellular carcinoma from Asia. *J. Clin. Oncol.* **2013**, *31*, 3501−3508.

(5) Zhao, X.; Liu, J.; Fan, J.; Chao, H.; Peng, X. Recent progress in photosensitizers for overcoming the challenges of photodynamic therapy: from molecular design to application. *Chem. Soc. Rev.* **2021**, *50*, 4185−4219.

(6) Li, X.; Lovell, J. F.; Yoon, J.; Chen, X. Clinical development and potential of photothermal and photodynamic therapies for cancer. *Nat. Rev. Clin. Oncol.* **2020**, *17*, 657−674.

(7) Lin, H.; Chen, Y.; Shi, J. Nanoparticle-triggered in situ catalytic chemical reactions for tumour-specific therapy. *Chem. Soc. Rev.* **2018**, *47*, 1938−1958.

(8) Li, K.; Xu, S.; Xiong, M.; Huan, S. Y.; Yuan, L.; Zhang, X. B. Molecular engineering of organic-based agents for in situ bioimaging and phototherapeutics. *Chem. Soc. Rev.* **2021**, *50*, 11766−11784.

(9) Fu, L. H.; Qi, C.; Lin, J.; Huang, P. Catalytic chemistry of glucose oxidase in cancer diagnosis and treatment. *Chem. Soc. Rev.* **2018**, *47*, 6454−6472.

(10) Liu, F.; Lin, L.; Zhang, Y.; Wang, Y.; Sheng, S.; Xu, C.; Tian, H.; Chen, X. A Tumor-Microenvironment-Activated Nanozyme-Mediated Theranostic Nanoreactor for Imaging-Guided Combined Tumor Therapy. *Adv. Mater.* **2019**, *31*, No. e1902885.

(11) Wang, P.; Shi, Y.; Zhang, S.; Huang, X.; Zhang, J.; Zhang, Y.; Si, W.; Dong, X. Hydrogen Peroxide Responsive Iron-Based Nanoplatform for Multimodal Imaging-Guided Cancer Therapy. *Small* **2019**, *15*, No. e1803791.

(12) Deng, L.; Liu, M.; Sheng, D.; Luo, Y.; Wang, D.; Yu, X.; Wang, Z.; Ran, H.; Li, P. Low-intensity focused ultrasound-augmented Cascade chemodynamic therapy via boosting ROS generation. *Biomaterials* **2021**, *271*, No. 120710.

(13) Zhou, Y.; Fan, S.; Feng, L.; Huang, X.; Chen, X. Manipulating Intratumoral Fenton Chemistry for Enhanced Chemodynamic and Chemodynamic-Synergized Multimodal Therapy. *Adv. Mater.* **2021**, *33*, No. e2104223.

(14) Zhang, L.; Zhang, K.; Wang, C.; Liu, Y.; Wu, X.; Peng, Z.; Cao, H.; Li, B.; Jiang, J. Advances and Prospects in Metal-Organic Frameworks as Key Nexus for Chemocatalytic Hydrogen Production. *Small* **2021**, *17*, No. e2102201.

(15) Wu, M. X.; Yang, Y. W. Metal-Organic Framework (MOF)-Based Drug/Cargo Delivery and Cancer Therapy. *Adv. Mater.* **2017**, *29*, No. 1606134.

(16) Shen, Y.; Pan, T.; Wang, L.; Ren, Z.; Zhang, W.; Huo, F. Programmable Logic in Metal-Organic Frameworks for Catalysis. *Adv. Mater.* **2021**, *33*, No. e2007442.

(17) Zheng, Q.; Liu, X.; Zheng, Y.; Yeung, K. W. K.; Cui, Z.; Liang, Y.; Li, Z.; Zhu, S.; Wang, X.; Wu, S. The recent progress on metal-organic frameworks for phototherapy. *Chem. Soc. Rev.* **2021**, *50*, 5086−5125.

(18) Zhang, Y.; Wang, L.; Liu, L.; Lin, L.; Liu, F.; Xie, Z.; Tian, H.; Chen, X. Engineering Metal-Organic Frameworks for Photoacoustic Imaging-Guided Chemo-/Photothermal Combinational Tumor Therapy. *ACS Appl. Mater. Interfaces* **2018**, *10*, 41035−41045.

(19) Cai, W.; Gao, H.; Chu, C.; Wang, X.; Wang, J.; Zhang, P.; Lin, G.; Li, W.; Liu, G.; Chen, X. Engineering Phototheranostic Nanoscale Metal-Organic Frameworks for Multimodal Imaging-Guided Cancer Therapy. *ACS Appl. Mater. Interfaces* **2017**, *9*, 2040−2051.

(20) Sheng, S.; Liu, F.; Lin, L.; Yan, N.; Wang, Y.; Xu, C.; Tian, H.; Chen, X. Nanozyme-mediated cascade reaction based on metal-organic framework for synergetic chemo-photodynamic tumor therapy. *J. Controlled Release* **2020**, *328*, 631−639.

(21) Fang, Y.; Yang, Z.; Li, H.; Liu, X. MIL-100(Fe) and its derivatives: from synthesis to application for wastewater decontamination. *Environ. Sci. Pollut. Res. Int.* **2020**, *27*, 4703−4724.

(22) Huang, R.; Yu, Y.; Zong, X.; Li, X.; Ma, L.; Zheng, Q. Monomethyltransferase SETD8 regulates breast cancer metabolism via stabilizing hypoxia-inducible factor 1alpha. *Cancer Lett.* **2017**, *390*, 1−10.

(23) Rottenberg, S.; Disler, C.; Perego, P. The rediscovery of platinum-based cancer therapy. *Nat. Rev. Cancer* **2021**, *21*, 37−50.

(24) Zhou, B.; Wu, Q.; Wang, M.; Hoover, A.; Wang, X.; Zhou, F.; Towner, R. A.; Smith, N.; Saunders, D.; Song, J.; Qu, J.; Chen, W. R. Immunologically modified MnFe(2)O(4) nanoparticles to synergize photothermal therapy and immunotherapy for cancer treatment. *Chem. Eng. J.* **2020**, *396*, No. 125239.
(25) Liu, T.; Liu, W.; Zhang, M.; Yu, W.; Gao, F.; Li, C.; Wang, S. B.; Feng, J.; Zhang, X. Z. Ferrous-Supply-Regeneration Nanoengineering for Cancer-Cell-Specific Ferroptosis in Combination with Imaging-Guided Photodynamic Therapy. *ACS Nano* **2018**, *12*, 12181−12192.
(26) Alcindor, T.; Beauger, N. Oxaliplatin: a review in the era of molecularly targeted therapy. *Curr. Oncol.* **2011**, *18*, 18−25.
(27) Shafirstein, G.; Bellnier, D.; Oakley, E.; Hamilton, S.; Potasek, M.; Beeson, K.; Parilov, E. Interstitial Photodynamic Therapy-A Focused Review. *Cancers* **2017**, *9*, 12.
(28) Lee, T. K.; Guan, X. Y.; Ma, S. Cancer stem cells in hepatocellular carcinoma - from origin to clinical implications. *Nat. Rev. Gastroenterol. Hepatol.* **2022**, *19*, 26−44.
(29) Petrowsky, H.; Fritsch, R.; Guckenberger, M.; De Oliveira, M. L.; Dutkowski, P.; Clavien, P. A. Modern therapeutic approaches for the treatment of malignant liver tumours. *Nat. Rev. Gastroenterol. Hepatol.* **2020**, *17*, 755−772.
(30) Kanat, O.; Ertas, H.; Caner, B. Platinum-induced neurotoxicity: A review of possible mechanisms. *World J. Clin. Oncol.* **2017**, *8*, 329−335.
(31) Avan, A.; Postma, T. J.; Ceresa, C.; Avan, A.; Cavaletti, G.; Giovannetti, E.; Peters, G. J. Platinum-induced neurotoxicity and preventive strategies: past, present, and future. *Oncologist* **2015**, *20*, 411−432.

https://doi.org/10.1021/acsami.2c19305
ACS Appl. Mater. Interfaces 2023, 15, 3781−3790